J. Fluid Mech. (2022), *vol*. 953, R1, doi:10.1017/jfm.2022.947

Inertial torque on a squirmer

F. Candelier[1], J. Qiu[2], L. Zhao[2], G. Voth[3] and B. Mehlig[4],†

[1]CNRS, IUSTI, Aix Marseille Univ, Marseille, France

[2]AML, Department of Engineering Mechanics, Tsinghua University, 100084 Beijing, PR China

[3]Department of Physics, Wesleyan University, Middletown, CT 06459, USA

[4]Department of Physics, Gothenburg University, 41296 Gothenburg, Sweden

(Received 7 September 2022; revised 5 November 2022; accepted 7 November 2022)

A small spheroid settling in a quiescent fluid experiences an inertial torque that aligns it so that it settles with its broad side first. Here we show that an active particle experiences such a torque too, as it settles in a fluid at rest. For a spherical squirmer, the torque is $\boldsymbol{T}' = -\frac{9}{8} m_f (\boldsymbol{v}_s^{(0)} \wedge \boldsymbol{v}_g^{(0)})$ where $\boldsymbol{v}_s^{(0)}$ is the swimming velocity, $\boldsymbol{v}_g^{(0)}$ is the settling velocity in the Stokes approximation and m_f is the equivalent fluid mass. This torque aligns the swimming direction against gravity: swimming up is stable, swimming down is unstable.

Key words: micro-organism dynamics

1. Introduction

The motion of small plankton in the turbulent ocean is overdamped (Visser 2011). Accelerations play no role, and hydrodynamic forces and torques can be computed in the Stokes approximation. Turbulence rotates these small organisms, yet they manage to navigate upwards towards the ocean surface. Gyrotactic organisms make use of gravity to achieve this. These bottom-heavy swimmers experience a gravity torque that tends to align against the direction of gravity, so that they swim upwards (Kessler 1985; Durham *et al.* 2013; Gustavsson *et al.* 2016). Also density or shape asymmetries give rise to torques in the Stokes approximation that can change the swimming direction (Roberts 1970; Jonsson 1989; Roberts & Deacon 2002; Candelier & Mehlig 2016; Roy *et al.* 2019).

Larger organisms accelerate the surrounding fluid as they move, and this changes the hydrodynamic force the swimmer experiences (Wang & Ardekani 2012; Khair & Chisholm 2014; Chisholm *et al.* 2016; Redaelli *et al.* 2022). Three different mechanisms cause such fluid-inertia effects: a non-zero slip velocity (Oseen problem with non-dimensional

† Email address for correspondence: bernhard.mehlig@physics.gu.se

parameter Re_p, the particle Reynolds number), velocity gradients of the disturbance flow (Saffman problem, shear Reynolds number Re_s) and unsteady fluid inertia (with parameter $Re_p\,Sl$, where Sl is the Strouhal number).

Fluid inertia gives rise to hydrodynamic torques. For a passive spheroid in spatially inhomogeneous flow, there are Re_s-corrections to Jeffery's torque (Subramanian & Koch 2005; Einarsson *et al.* 2015; Rosén *et al.* 2015; Dabade, Marath & Subramanian 2016; Marath & Subramanian 2018). A passive spheroid settling in a quiescent fluid experiences an inertial torque, a Re_p-effect. This Khayat-Cox torque tends to align the particle so that it settles with its broad side down (Brenner 1961; Cox 1965; Khayat & Cox 1989; Klett 1995; Dabade, Marath & Subramanian 2015; Kramel 2017; Lopez & Guazzelli 2017; Menon *et al.* 2017; Gustavsson *et al.* 2019; Jiang *et al.* 2021; Cabrera *et al.* 2022). For a passive sphere, spherical symmetry ensures that the Khayat-Cox torque vanishes.

In this paper, we show that a small spherical squirmer experiences an inertial torque analogous to the Khayat & Cox torque when it settles in a quiescent fluid. Using asymptotic matching, we calculate the torque to leading order in the particle Reynolds number

$$Re_p = au_c/\nu, \tag{1.1}$$

where u_c is a velocity scale, a is the radius of the squirmer and ν is the kinematic viscosity of the fluid. The calculation shows that the inertial torque does not vanish for a spherical swimmer because swimming breaks rotational symmetry. We describe how the torque aligns the squirmer, and compare its effect with gyrotactic torques, and with the Khayat-Cox torque for a non-spherical passive particle.

2. Model

We consider a steady spherical squirmer, an idealised model for a motile micro-organism developed by Lighthill (1952) and Blake (1971). In this model, one imposes an active axisymmetric tangential surface-velocity field of the form

$$(B_1 \sin\theta + B_2 \sin\theta\cos\theta)\hat{\boldsymbol{e}}_\theta, \tag{2.1}$$

with parameters B_1 and B_2, and where θ is the angle between the swimming direction (unit vector $\boldsymbol{n}$) and the vector $\boldsymbol{r}$ from the particle centre to a point on its surface. The tangential unit vector at this point is denoted by $\hat{\boldsymbol{e}}_\theta$. One distinguishes two types of squirmers depending on the parameter $\beta = B_2/B_1$ (Lauga & Powers 2009): 'pushers' ($\beta < 0$) and 'pullers' with $\beta > 0$. In the Stokes limit, a squirmer moving with velocity $\dot{\boldsymbol{x}}$ in a fluid at rest experiences the hydrodynamic force

$$\boldsymbol{F}'^{(0)} = 6\pi\varrho_f \nu a \left(\tfrac{2}{3}B_1\boldsymbol{n} - \dot{\boldsymbol{x}}\right). \tag{2.2}$$

Here the superscript denotes the Stokes approximation, and ϱ_f is the mass density of the fluid. Following Candelier, Mehlig & Magnaudet (2019) and Candelier *et al.* (2022), we use a prime to indicate that this is the hydrodynamic force on the squirmer, due to the disturbance it creates.

Plankton tends to be slightly heavier than the fluid. Therefore we allow the squirmer to settle subject to the buoyancy force

$$\boldsymbol{F}_g = \frac{4\pi}{3}a^3(\varrho_s - \varrho_f)\boldsymbol{g}, \tag{2.3}$$

where ϱ_s is the mass density of the squirmer, and $\boldsymbol{g}$ is the gravitational acceleration. In the overdamped limit, the steady centre-of-mass velocity of the squirmer is determined by

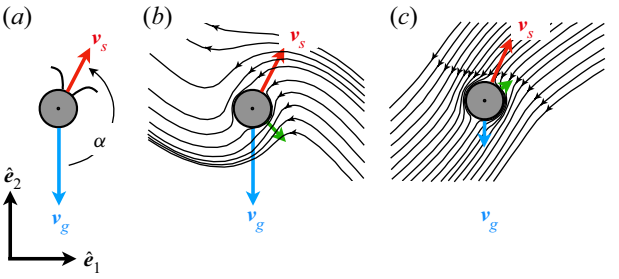

Figure 1. (*a*) Squirmer with swimming velocity $\boldsymbol{v}_s$ and settling velocity $\boldsymbol{v}_g$, see § 2. Gravity points in the negative $\hat{\boldsymbol{e}}_2$-direction. (*b*,*c*) Disturbance flow created by a squirmer with $B_2 = 0$ (schematic). Shown are the flow lines in the frame that translates with the body. The centre-of-mass velocity $\dot{\boldsymbol{x}}$ is shown in green.

the zero-force condition $\boldsymbol{F}'^{(0)} + \boldsymbol{F}_g = \boldsymbol{0}$. This yields $\dot{\boldsymbol{x}} = \frac{2}{3}B_1\boldsymbol{n} + \frac{2}{9}(\varrho_s/\varrho_f - 1)(a^2/\nu)\boldsymbol{g} \equiv \boldsymbol{v}_s^{(0)} + \boldsymbol{v}_g^{(0)}$. Again, the superscript denotes the Stokes limit. In this limit, the squirmer experiences no torque in a fluid at rest, $\boldsymbol{T}'^{(0)} = \boldsymbol{0}$.

3. Inertial torque

Assume that the squirmer swims with swimming velocity $\boldsymbol{v}_s$ and settles with settling velocity $\boldsymbol{v}_g$. The angle between $\boldsymbol{v}_s$ and $\boldsymbol{v}_g$ is denoted by α, as shown in figure 1(*a*). Symmetry dictates the form of the inertial torque $\boldsymbol{T}'$. It has the units mass $\times$ velocity^2. Since the torque is an axial vector, it must be proportional to the vector product between the two velocities. The torque can therefore be written as

$$\boldsymbol{T}'^{(1)} = Cm_f(\boldsymbol{v}_s \wedge \boldsymbol{v}_g), \tag{3.1}$$

where $m_f = (4\pi/3)a^3\varrho_f$ is the equivalent fluid mass, C is a non-dimensional constant, and the superscript indicates that this is the first inertial correction to the torque. Equation (3.1) says that torque vanishes when the swimmer swims against gravity ($\alpha = \pi$ in figure 1*a*), and when it swims in the direction of gravity ($\alpha = 0$). Bifurcation theory implies that one of these fixed points is stable, the other one unstable. The sign of the coefficient C determines which of the two is the stable fixed point.

Inertial torques can be understood as a consequence of advection of fluid momentum. In the frame translating with the squirmer, far-field momentum is advected by the transverse disturbance flow generated by the squirmer, as illustrated schematically in figure 1(*b*,*c*). At non-zero Re_p, the head of the squirmer – the north pole of the axial velocity field (2.1) – experiences more drag than its rear, because some of the momentum imparted to the fluid by the head is advected to the trailing end, in the direction transverse to gravity. So when $\boldsymbol{v}_s$ is not co-linear with $\boldsymbol{v}_g$ there is an inertial torque which rotates the swimmer so that $\boldsymbol{v}_s$ becomes closer to anti-parallel with $\boldsymbol{v}_g$. Comparing with (3.1), this means that the coefficient C must be negative. Note that the mechanism described above is the same that creates Khayat-Cox torques on non-spherical passive particles sedimenting in quiescent fluid. For a fibre, for example, the far-field momentum is advected by the transverse flow along the fibre, leading to a torque that aligns the fibre perpendicular to gravity (Khayat & Cox 1989).

4. Perturbation theory for the coefficient C

The inertial torque is computed from

$$\boldsymbol{T}'^{(1)} = \int_{\mathscr{S}} \boldsymbol{r} \wedge (\varpi^{(1)}\,\mathrm{d}\boldsymbol{s}), \tag{4.1}$$

where $\sigma^{(1)}_{mn} = -p^{(1)}\delta_{mn} + 2\mu S^{(1)}_{mn}$ are the elements of the stress tensor $\varpi^{(1)}$ with pressure $p^{(1)}$, $S^{(1)}_{mn}$ are the elements of the strain-rate tensor of the disturbance flow and $\mu = \varrho_f \nu$ is the dynamic viscosity. The integral goes over the particle surface $\mathscr{S}$, $\boldsymbol{r}$ is the vector from the particle centre to a point on the particle surface and $\mathrm{d}\boldsymbol{s}$ is the outward surface normal at this point. In the Stokes approximation the torque vanishes, $\boldsymbol{T}'^{(0)} = \boldsymbol{0}$, as mentioned above.

The disturbance stress tensor is determined by solving the steady Navier–Stokes equations for the velocity $\boldsymbol{w}$ of the incompressible disturbance flow caused by the squirmer,

$$-Re_p\dot{\boldsymbol{x}}\cdot\boldsymbol{\nabla}\boldsymbol{w} + Re_p\boldsymbol{w}\cdot\boldsymbol{\nabla}\boldsymbol{w} = -\boldsymbol{\nabla}p + \boldsymbol{\Delta}\boldsymbol{w}, \tag{4.2}$$

with boundary conditions $\boldsymbol{w} = \dot{\boldsymbol{x}} + (B_1\sin\theta + B_2\sin\theta\cos\theta)\hat{\boldsymbol{e}}_\theta$ for $|\boldsymbol{r}| = 1$, and $\boldsymbol{w} \to \boldsymbol{0}$ as $|\boldsymbol{r}| \to \infty$. Here we assumed that the squirmer has no angular velocity. We non-dimensionalised (4.2) using the radius a of the squirmer as a length scale, and with the velocity scale $u_c = v_g^{(0)}$. Forces are non-dimensionalised by $\mu a u_c$, and torques by $\mu a^2 u_c$. The acceleration terms on the left-hand side of (4.2) are singular perturbations of the right-hand side, the Stokes part. We use matched asymptotic expansions in Re_p to determine the solution for small Re_p (Hinch 1995). Near the squirmer, one expands:

$$\boldsymbol{w}_{in} = \boldsymbol{w}^{(0)}_{in} + Re_p\boldsymbol{w}^{(1)}_{in} + \cdots \quad \text{and} \quad p_{in} = p^{(0)}_{in} + Re_p p^{(1)}_{in} + \cdots . \tag{4.3a,b}$$

This inner expansion is matched, term by term, to an outer expansion:

$$\hat{\boldsymbol{w}}_{out} = \hat{\mathcal{T}}^{(0)}_{reg} + Re_p(\hat{\mathcal{T}}^{(1)}_{reg} + \hat{\mathcal{T}}^{(1)}_{sing}) + \cdots . \tag{4.4}$$

Here $\hat{\mathcal{T}}^{(0,1)}_{reg}$ are regular terms in the outer expansion, while $\hat{\mathcal{T}}^{(1)}_{sing}$ is singular in $\boldsymbol{k}$-space, proportional to $\delta(\boldsymbol{k})$ (Meibohm *et al.* 2016). The outer solution is obtained by replacing the boundary condition on the surface of the squirmer by a singular source term in (4.2), a Dirac δ-function with amplitude $\boldsymbol{F}^{(0)} = -6\pi(\frac{2}{3}B_1\boldsymbol{n} - \dot{\boldsymbol{x}})$. Since the non-linear term (quadratic in $\boldsymbol{w}$) is negligible far from the particle, the resulting equation can be solved by Fourier transform, yielding explicit expressions for $\hat{\mathcal{T}}^{(0,1)}_{reg}$ and $\hat{\mathcal{T}}^{(1)}_{sing}$ which serve as boundary conditions for the inner problems. The inner problem to order Re_p^0 is the homogeneous Stokes problem

$$-\boldsymbol{\nabla}p^{(0)}_{in} + \boldsymbol{\Delta}\boldsymbol{w}^{(0)}_{in} = \boldsymbol{0}, \quad \boldsymbol{\nabla}\cdot\boldsymbol{w}^{(0)}_{in} = \boldsymbol{0}, \tag{4.5a}$$

with boundary conditions

$$\boldsymbol{w}^{(0)}_{in} = \dot{\boldsymbol{x}} + (B_1\sin\theta + B_2\sin\theta\cos\theta)\hat{\boldsymbol{e}}_\theta \quad \text{for } |\boldsymbol{r}| = 1, \quad \boldsymbol{w}^{(0)}_{in} \sim \mathcal{T}^{(0)}_{reg} \quad \text{as } |\boldsymbol{r}| \to \infty. \tag{4.5b}$$

This problem is solved in the standard fashion using Lamb's solution (Happel & Brenner 1965). The Re_p^1-order inner problem is inhomogeneous:

$$-\boldsymbol{\nabla}p^{(1)}_{in} + \boldsymbol{\Delta}\boldsymbol{w}^{(1)}_{in} = -Re_p\dot{\boldsymbol{x}}\cdot\boldsymbol{\nabla}\boldsymbol{w}^{(0)}_{in} + Re_p\boldsymbol{w}^{(0)}_{in}\cdot\boldsymbol{\nabla}\boldsymbol{w}^{(0)}_{in}, \quad \boldsymbol{\nabla}\cdot\boldsymbol{w}^{(1)}_{in} = 0, \tag{4.6a}$$

$$\boldsymbol{w}^{(1)}_{in} = \boldsymbol{0} \quad \text{for } |\boldsymbol{r}| = 1 \quad \text{and} \quad \boldsymbol{w}^{(1)}_{in} \sim \mathcal{T}^{(1)}_{reg} + \mathcal{T}^{(1)}_{sing} \quad \text{for } |\boldsymbol{r}| \to \infty. \tag{4.6b}$$

To solve (4.6), we make the ansatz $\boldsymbol{w}_{in}^{(1)} = (\boldsymbol{w}_p + \mathcal{T}_{sing}^{(1)}) + \boldsymbol{w}_h$, where $\boldsymbol{w}_p$ is a particular solution and $\boldsymbol{w}_h$ is the homogeneous solution of (4.6*a*). For the pressure we write $p_{in}^{(1)} = p_p^{(1)} + p_h^{(1)}$. We first determine the particular solution $\boldsymbol{w}_p^{(1)}$ and $p_p^{(1)}$ by Fourier transform, as described in Candelier *et al.* (2022). Then $\boldsymbol{w}_h^{(1)}$ and $p_h^{(1)}$ are determined using Lamb's solution. The boundary condition for $\boldsymbol{w}_h$ is $\boldsymbol{w}_h^{(1)} = -\boldsymbol{w}_p^{(1)} - \mathcal{T}_{sing}^{(1)}$ on the particle surface. Having obtained $\boldsymbol{w}_{in}^{(1)}$, we compute the torque from (4.1). The torque comes from the particular solution of the first-order inner problem; there are no singular contributions at this order. Note also that for a passive spherical particle, spherical symmetry ensures that the particular solution does not contribute to the torque. Swimming breaks spherical symmetry, and this is the reason that torque does not vanish for a spherical squirmer. Given $p^{(1)}$ and $\boldsymbol{w}_{in}^{(1)}$, we can determine the inertial correction $\varpi^{(1)}$ to the stress tensor. Performing the integral in (4.1), we find the leading-order contribution to the torque,

$$\boldsymbol{T}'^{(1)} = -\frac{3\pi}{2} Re_p (\boldsymbol{v}_s^{(0)} \wedge \boldsymbol{v}_g^{(0)}). \tag{4.7}$$

In dimensional units, this corresponds to $\boldsymbol{T}'^{(1)} = -\frac{9}{8} m_f (\boldsymbol{v}_s^{(0)} \wedge \boldsymbol{v}_g^{(0)})$. The coefficient $C = -\frac{9}{8}$ is negative, as predicted by the argument summarised in § 3. So a spherical organism swimming downwards experiences a torque that tends to turn it upwards, causing the organism to swim against gravity.

5. Direct numerical simulations

We solved the three-dimensional Navier–Stokes equations for the incompressible flow using an immersed-boundary method (Peskin 2002). The interaction between squirmer and fluid was implemented by the direct-force method (Uhlmann 2005): to satisfy the boundary condition (2.1), the algorithm calculates the predicted fluid velocity on the surface of the squirmer. Based on the mismatch between the predicted velocity and (2.1), an appropriate immersed-boundary force is applied to the fluid phase to maintain the boundary conditions (2.1) on the surface of the squirmer. We used the improved algorithm of Kempe & Fröhlich (2012), Breugem (2012) and Lambert *et al.* (2013), because it is more precise for nearly neutrally buoyant particles. We used a cubic computational domain of side length $L = 20a$ with periodic boundary conditions. The computational domain was discretised using a cubic mesh with resolution Δx. The Navier–Stokes equations were integrated using a second-order Crank-Nicholson scheme (Kim, Baek & Sung 2002) with time step Δt, while the motion of the squirmer was integrated using a second-order Adams–Bashforth method. The numerical simulation of solid-body motion in a fluid is challenging at small Re_p. The mesh resolution Δx must be fine enough to resolve the shape of the body, so that the viscous stresses near its surface are accurately represented. In addition, the time step Δt must be small enough to resolve the viscous diffusion of the disturbance, $\Delta t < \Delta x^2/\nu$ (Appendix).

To determine the torque, we froze the orientation of the squirmer at a given angle α, but allowed the squirmer to translate. It was initially at rest. We measured the centre-of-mass velocity and the torque after the transient, when the disturbance flow was fully established. Figure 2(*a*) shows the numerical results for the inertial torque on a spherical squirmer for different values of Re_p, in comparison with the theory (4.7). The remaining parameter values used in the simulations are quoted in the caption for figure 2. We see that the simulation results approach the small-Re_p theory as the particle Reynolds number

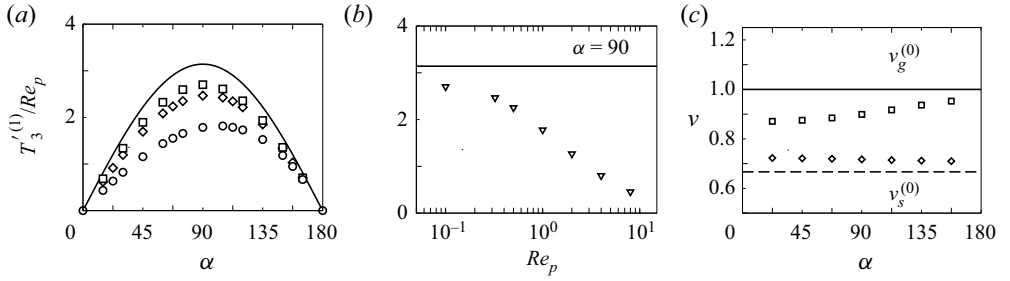

Figure 2. (*a*) Non-dimensional inertial torque $\boldsymbol{T}'^{(1)} = T_3'^{(1)}\hat{\boldsymbol{e}}_3$ on a spherical squirmer. Shown is the theory, (4.7) (solid line), in comparison with direct numerical simulation results (§ 5) for different values of particle Reynolds number: $Re_p = 0.1$ (□), $Re_p = 0.323$ (◊) and $Re_p = 1$ (○). The torque was non-dimensionalised by $\mu a^2 u_c$, where $u_c = v_g^{(0)}$. The angle α is defined in figure 1(*a*). Parameters: $B_1 = 1$, $B_2 = 0$, $v_s^{(0)} = 2/3$, $v_g^{(0)} = 1$. Mesh resolution $2a/\Delta x = 36$, time step $\nu\Delta t/\Delta x^2 = 0.22$. (*b*) Non-dimensional torque for $\alpha = 90$ as a function of Re_p; other parameters same as in (*a*). Also shown is (4.7). (*c*) Non-dimensional swimming speed (◇) and settling speed (□) from direct numerical simulations for $Re_p = 0.323$; other parameters same as in (*a*). Also shown are the Stokes estimates $v_s^{(0)}$ (dashed) and $v_g^{(0)}$ (solid).

decreases. For the smallest value of Re_p we simulated, $Re_p = 0.1$, the relative error is approximately 16 %. For $Re_p = 1$, the difference is much larger, but the simulation results nevertheless agree qualitatively with the small-Re_p theory. This is encouraging, because it allows us to draw qualitative conclusions about the effects of the torque on plankton (§ 6). We note, however, that the numerical results for $Re_p = 1$ exhibit an asymmetry in their dependence on α. Since the small-Re_p theory yields a symmetric angular dependence of the torque, we attribute the asymmetry to higher-order Re_p-corrections.

The small-Re_p theory predicts that $T_3'^{(1)}/Re_p$ approaches a Re_p-independent plateau as $Re_p \to 0$. Figure 2(*b*) indicates that this plateau is not yet reached for $Re_p = 0.1$. We note that there is still a residual time-step dependence for $Re_p = 0.1$. Decreasing the time step further from $\nu\Delta t/\Delta x^2 = 0.22$ to 0.11 increases the numerical value by 2.4 %. The deviation between the small-Re_p theory and the simulation result of 16 % at $Re_p = 0.1$ is consistent with that of Jiang *et al.* (2021), who numerically computed the Khayat-Cox torque for settling spheroids, and found that the simulation result is approximately 20 % lower at $Re_p \approx 0.3$ than the small-Re_p theory. Kharrouba, Pierson & Magnaudet (2021) found smaller differences for a slender cylinder settling in a quiescent fluid, between 8 % and 13 % for $Re_p = 0.05$, depending on the orientation of the cylinder. Note, however, that they compared with the more precise slender-body theory ((6.13) in Khayat & Cox 1989). This approximation is more accurate as Re_p grows than (6.22) in Khayat & Cox (1989) which is the equivalent of (4.7) here.

Another indication that higher-order Re_p-corrections are important comes from measuring settling and swimming speeds in the numerical simulations. We extracted the swimming speed using $\dot{\boldsymbol{x}} = v_s\boldsymbol{n} - v_g\hat{\boldsymbol{e}}_2$. Solving for v_s gives $v_s = \dot{\boldsymbol{x}}\cdot\hat{\boldsymbol{e}}_1/(\boldsymbol{n}\cdot\hat{\boldsymbol{e}}_1)$. Figure 2(*c*) shows the measured swimming and settling speeds at $Re_p = 0.323$. The settling speed is substantially smaller than the Stokes estimate, consistent with a significant Re_p-correction. The swimming speed is much closer to the Stokes estimate. This is because the data shown is for $\beta = 0$, and the known Re_p-corrections to the swimming speed (Khair & Chisholm 2014),

$$\boldsymbol{v}_s = \frac{2}{3}B_1\boldsymbol{n}\left[1 - \frac{3\beta}{20}Re_p + \left(\frac{\beta}{8} + \frac{11\,987}{470\,400}\beta^2\right)Re_p^2 + \cdots\right], \tag{5.1}$$

vanish for $\beta = 0$. We note that the numerical results of Chisholm *et al.* (2016) indicate that $\boldsymbol{v}_s$ does not depend on Re_p at all for $\beta = 0$.

6. Conclusions

We showed that a spherical squirmer settling in a fluid at rest experiences an inertial torque, and computed the torque using matched asymptotic expansions. The calculation is similar to that of Cox (1965) for the inertial torque on a nearly spherical, passive particle settling in a quiescent fluid. This torque vanishes for a passive sphere, a consequence of spherical symmetry. A spherical swimmer experiences an inertial torque because swimming breaks this symmetry. The torque causes the squirmer to align with gravity so that it swims upwards. In other words, this torque acts just like Kessler's gyrotactic torque for bottom-heavy organisms.

For small plankton, the effect of the inertial torque is much smaller than the gyrotactic torque, at least for spherical shapes. We can see this by comparing the corresponding reorientation times. This time scale is defined as $\tau_I = \frac{1}{2}(8\pi\mu a^3)/T_{max}$, where $8\pi\mu a^3$ is the rotational resistance coefficient for a sphere (Kim & Karrila 2013) and T_{max} is the maximal magnitude of the torque. For the inertial torque, one obtains $\tau_I = 8\nu/(3v_s^{(0)}v_g^{(0)})$ (this and all following expressions are quoted in dimensional units). The reorientation time for the gyrotactic torque is $\tau_G = 3\varrho_s\nu/(\varrho_f g h)$ (Pedley & Kessler 1987), where h is the offset between the centre-of-mass and the geometrical centre of the squirmer, and $g = |\boldsymbol{g}|$. The ratio of these time scales is $\tau_I/\tau_G \sim gh/v_s^{(0)}v_g^{(0)}$, assuming $\varrho_s \approx \varrho_f$. Taking $h \sim 10^{-7}\,\mathrm{m}$ (table 1 in Kessler 1986), we see that swimming and settling speeds need to be of the order of $\mathrm{mm\,s^{-1}}$ for the reorientation times to be comparable. For small plankton, typical speeds tend to be much smaller (Kessler 1986).

For larger organisms, however, the inertial torque can be significant. With typical values for a copepod (Titelman & Kiørboe 2003), $v_s = 1$, $v_g = 0.2\,\mathrm{mm\,s^{-1}}$, as well as $\nu = 10^{-6}\,\mathrm{m^2\,s^{-1}}$, one finds an inertial reorientation time of the order of $\tau_I \sim 10\,\mathrm{s^{-1}}$. Kolmogorov times for ocean turbulence range from $\tau_K = \sqrt{\nu/\mathscr{E}} = 100\,\mathrm{s}$ for dissipation rate per unit mass $\mathscr{E} = 10^{-6}\,\mathrm{cm^2\,s^{-3}}$ to $\tau_K = 1\,\mathrm{s}$ for $\mathscr{E} = 10^{-2}\,\mathrm{cm^2\,s^{-3}}$. So the non-dimensional reorientation parameter $\Psi = \tau_I/\tau_K$ (Durham *et al.* 2013) ranges from 0.1 for weak turbulence to 10 for strong turbulence. The Reynolds number is of order $\mathrm{Re}_p \sim 1$ for speeds of the order of 1 mm, so that the Re_p-perturbation theory does not strictly apply. However, since the theory works qualitatively as we demonstrated above, we can nevertheless conclude that for weak turbulence, the inertial torque can have a significant effect on the angular dynamics of the organism.

Some motile micro-organisms are non-spherical (Berland, Maestrini & Grzebyk 1995; Faust & Gulledge 2002; Smayda 2010). It has been suggested that a non-spherical settling squirmer experiences an inertial Khayat-Cox torque (Qiu *et al.* 2022). Since the boundary conditions differ between passive and active particles, and since swimming breaks fore-aft symmetry, the inertial torque on a non-spherical squirmer may be different from the Khayat-Cox torque. However, we expect that the torque is still determined by the same physical mechanism, advection of fluid-momentum transverse to gravity. This may give rise to terms proportional to $\sin(2\alpha)$, whereas the torque is proportional to $\sin(\alpha)$ for the spherical squirmer. To make these speculations definite, one could compute the inertial torque for a nearly spherical squirmer in perturbation theory. A second open question is to determine the inertial torque for bottom-heavy, non-spherical organisms, the analogue of the inertial torque on passive particles with mass-density asymmetries (Roy *et al.* 2019).

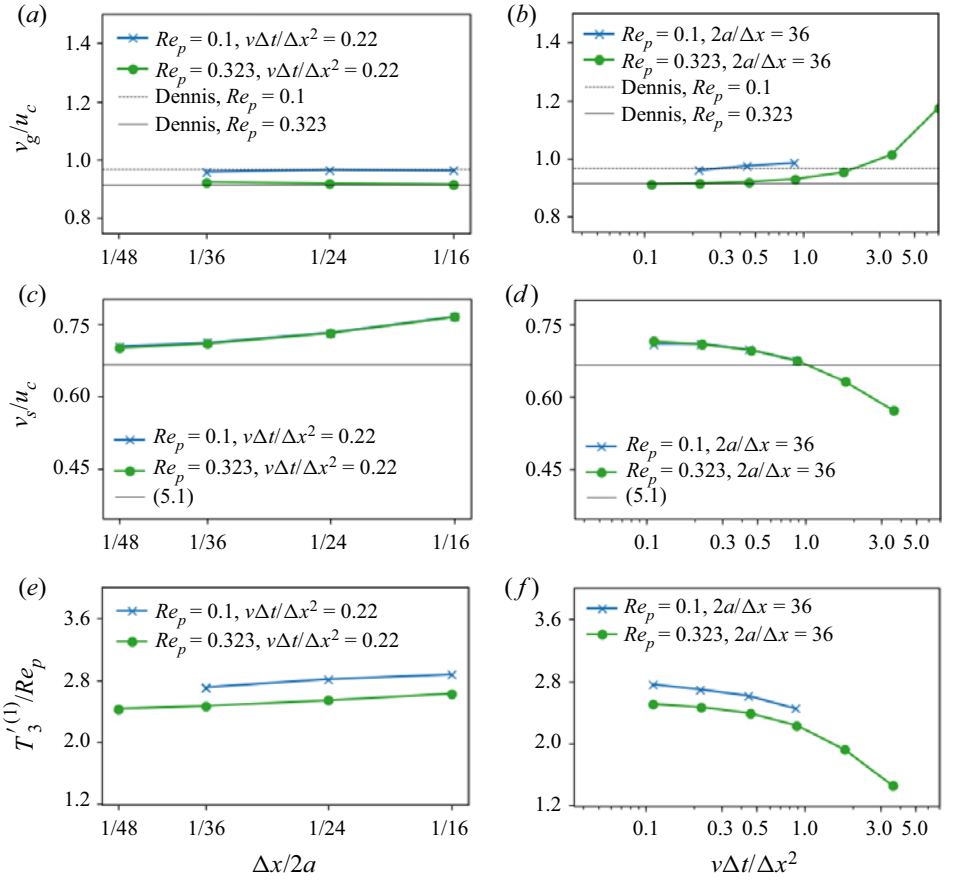

Figure 3. Convergence tests changing mesh resolution Δx (*a*,*c*,*e*) and changing integration time step Δt (*b*,*d*,*f*). Settling speed of a passive sphere (*a*,*b*), compared with the numerical data of Dennis & Walker (1971), extracted from figure 4 of Vesey & Goldenfeld (2007). Swimming speed of neutrally buoyant spherical squirmer with $\beta = 0$, compared with (5.1), (Khair & Chisholm 2014), (*c*,*d*). Panels (*e*,*f*) show the inertial torque.

More generally, although the small-Re_p perturbation theory may become quantitatively inaccurate for Reynolds numbers of order unity – where the torque begins to make a significant difference – the results tell us which non-dimensional parameters matter, and how to reason about the effect of boundary conditions, and the symmetries of the problem. The calculation illustrates the conceptual insight that the inertial torque comes from fluid motion transverse to the direction of gravity. Fluid momentum in this direction is advected along the swimmer by the transverse fluid velocity, resulting in a torque. In our case, the boundary conditions are different from those for passive particles, and so is the symmetry of the problem, because swimming breaks fore-aft symmetry. Nevertheless, the fundamental mechanism generating the torque is the same.

Funding. B.M. was supported by Vetenskapsrådet (grant no. 2021-4452) and by the Knut-and-Alice Wallenberg Foundation (grant no. 2019.0079). L.Z. was supported by the National Natural Science Foundation of China (grant nos. 11911530141 and 91752205). This research was also supported in part by a collaboration grant from the joint China-Sweden mobility programme [National Natural Science Foundation of China (NSFC)-Swedish Foundation for International Cooperation in Research and Higher Education (STINT)], grant nos. 11911530141 (NSFC) and CH2018-7737 (STINT).

Declaration of interests. The authors report no conflict of interest.

Author ORCIDs.
F. Candelier https://orcid.org/0000-0003-4826-1915;
J. Qiu https://orcid.org/0000-0003-0064-3797;
L. Zhao https://orcid.org/0000-0002-3642-3051;
G. Voth https://orcid.org/0000-0002-4443-8341;
B. Mehlig https://orcid.org/0000-0002-3672-6538.

Appendix. Details regarding the direct numerical simulations

This Appendix describes how we found the required mesh and time resolutions for our numerical simulations. We considered two test cases: a passive sphere settling under gravity, and a neutrally buoyant squirmer with $\beta = 0$, $Re_p = 0.1$ and 0.323. To check convergence as the mesh resolution increases, we changed $\Delta x/2a$, keeping $\nu\Delta t/\Delta x^2 = 0.22$ constant. Settling and swimming speeds reached a plateau when we increased the mesh resolution (left column of figure 3). For $Re_p = 0.323$, the settling speed varied by 1.1 % and the swimming speed varied by 1.3 % when we changed $\Delta x/2a$ from 1/36 to 1/48.

We then checked for convergence as the step size Δt was reduced, for fixed $\Delta x/2a = 1/36$. Again, both settling and swimming speeds reached plateaus as $\nu\Delta t/\Delta x^2$ decreased (right column of figure 3). For $Re_p = 0.323$, when we halved $\nu\Delta t/\Delta x^2$ from 0.22 to 0.11, the settling and swimming speeds varied by 0.25 % and 0.79 %, respectively. Therefore, we used $\Delta x/2a = 1/36$ and $\Delta t = 0.22\Delta x^2/\nu$ for most of the numerical simulations discussed in the main text. At these parameter values, the simulated settling speed of a passively settling particle is approximately 1 % larger than the numerical calculation of Dennis & Walker (1971), taken from figure 4 of Vesey & Goldenfeld (2007). The swimming speed of the squirmer is independent of Re_p in the range [0.1, 1], and it is 6.3 % larger than the theoretical value $v_s^{(0)} = 2B_1/3$. This error constrains the overall accuracy of the numerical method; it is slightly less accurate for the active compared with the passive particle.

Finally, consider the torque (bottom panels of figure 3). For $Re_p = 0.323$, the torque varied by approximately 1.5 % when we changed $\Delta x/2a$ from 1/36 to 1/48 for $\nu\Delta t/\Delta x^2 = 0.22$, and it varied by 1.6 % when we halved $\nu\Delta t/\Delta x^2$ from 0.22 to 0.11 for $\Delta x/2a = 1/36$.

References

Berland, B.R., Maestrini, S.Y. & Grzebyk, D. 1995 Observations on possible life cycle stages of the dinoflagellates Dinophysis cf. acuminata, Dinophysis acuta and Dinophysis pavillardi. *Aquat. Microb. Ecol.* **9** (2), 183–189.

Blake, J.R. 1971 A spherical envelope approach to ciliary propulsion. *J. Fluid Mech.* **46**, 199–208.

Brenner, H. 1961 The Oseen resistance of a particle of arbitrary shape. *J. Fluid Mech.* **11**, 604–610.

Breugem, W.-P. 2012 A second-order accurate immersed boundary method for fully resolved simulations of particle-laden flows. *J. Comput. Phys.* **231** (13), 4469–4498.

Cabrera, F., Sheikh, M.Z., Mehlig, B., Plihon, N., Bourgoin, M., Pumir, A. & Naso, A. 2022 Experimental validation of fluid inertia models for a cylinder settling in a quiescent flow. *Phys. Rev. Fluids* **7**, 024301.

Candelier, F., Mehaddi, R., Mehlig, B. & Magnaudet, J. 2022 Second-order inertial forces and torques on a sphere in a viscous steady linear flow. arXiv:2208.11565.

Candelier, F. & Mehlig, B. 2016 Settling of an asymmetric dumbbell in a quiescent fluid. *J. Fluid Mech.* **802**, 174–185.

CANDELIER, F., MEHLIG, B. & MAGNAUDET, J. 2019 Time-dependent lift and drag on a rigid body in a viscous steady linear flow. *J. Fluid Mech.* **864**, 554–595.

CHISHOLM, N.G., LEGENDRE, D., LAUGA, E. & KHAIR, A.S. 2016 A squirmer across Reynolds numbers. *J. Fluid Mech.* **796**, 233–256.

COX, R.G. 1965 The steady motion of a particle of arbitrary shape at small Reynolds numbers. *J. Fluid Mech.* **23**, 625–643.

DABADE, V., MARATH, N.K. & SUBRAMANIAN, G. 2015 Effects of inertia and viscoelasticity on sedimenting anisotropic particles. *J. Fluid Mech.* **778**, 133–188.

DABADE, V., MARATH, N.K. & SUBRAMANIAN, G. 2016 The effect of inertia on the orientation dynamics of anisotropic particles in simple shear flow. *J. Fluid Mech.* **791**, 631–703.

DENNIS, S.C.R & WALKER, J.D.A. 1971 Calculation of the steady flow past a sphere at low and moderate Reynolds numbers. *J. Fluid Mech.* **48**, 771–789.

DURHAM, W.M., CLIMENT, E., BARRY, M., LILLO, F.D., BOFFETTA, G., CENCINI, M. & STOCKER, R. 2013 Turbulence drives microscale patches of motile phytoplankton. *Nat. Commun.* **4**, 2148.

EINARSSON, J., CANDELIER, F., LUNDELL, F., ANGILELLA, J.R. & MEHLIG, B. 2015 Rotation of a spheroid in a simple shear at small Reynolds number. *Phys. Fluids* **27**, 063301.

FAUST, M.A. & GULLEDGE, R.A. 2002 Identifying harmful marine dinoflagellates. *Contr. U. S. Natl. Herb.* **42**, 1–144.

GUSTAVSSON, K., BERGLUND, F., JONSSON, P.R. & MEHLIG, B. 2016 Preferential sampling and small-scale clustering of gyrotactic microswimmers in turbulence. *Phys. Rev. Lett.* **116**, 108104.

GUSTAVSSON, K., SHEIKH, M.Z., LOPEZ, D., NASO, A., PUMIR, A. & MEHLIG, B. 2019 Theory for the effect of fluid inertia on the orientation of a small spheroid settling in turbulence. *New J. Phys.* **21**, 083008.

HAPPEL, J. & BRENNER, H. 1965 *Low Reynolds Number Hydrodynamics: With Special Applications to Particulate Media*. Prentice-Hall.

HINCH, E.J. 1995 *Perturbation Methods*. Cambridge University Press.

JIANG, F., ZHAO, L., ANDERSSON, H.I., GUSTAVSSON, K., PUMIR, A. & MEHLIG, B. 2021 Inertial torque on a small spheroid in a stationary uniform flow. *Phys. Rev. Fluids* **6**, 024302.

JONSSON, P.R. 1989 Vertical distribution of planktonic ciliates - an experimental analysis of swimming behaviour. *Mar. Ecol. Prog. Ser.* **52**, 39–53.

KEMPE, T. & FRÖHLICH, J. 2012 An improved immersed boundary method with direct forcing for the simulation of particle laden flows. *J. Comput. Phys.* **231** (9), 3663–3684.

KESSLER, J.O. 1985 Hydrodynamic focusing of motile algal cells. *Nature* **313**, 218–220.

KESSLER, J.O. 1986 Individual and collective fluid dynamics of swimming cells. *J. Fluid Mech.* **173**, 191–205.

KHAIR, A.S. & CHISHOLM, N.G. 2014 Expansions at small Reynolds numbers for the locomotion of a spherical squirmer. *Phys. Fluids* **26** (1), 011902.

KHARROUBA, M., PIERSON, J.-L. & MAGNAUDET, J. 2021 Flow structure and loads over inclined cylindrical rodlike particles and fibers. *Phys. Rev. Fluids* **6**, 044308.

KHAYAT, R.E. & COX, R.G. 1989 Inertia effects on the motion of long slender bodies. *J. Fluid Mech.* **209**, 435–462.

KIM, K., BAEK, S.-J. & SUNG, H.J. 2002 An implicit velocity decoupling procedure for the incompressible Navier–Stokes equations. *Intl J. Numer. Meth. Fluids* **38**, 125–138.

KIM, S. & KARRILA, S.J. 2013 *Microhydrodynamics: Principles and Selected Applications*. Courier Corporation.

KLETT, J.D. 1995 Orientation model for particles in turbulence. *J. Atmos. Sci.* **52**, 2276–2285.

KRAMEL, S. 2017 Non-spherical particle dynamics in turbulence. PhD thesis, Wesleyan University.

LAMBERT, R.A., PICANO, F., BREUGEM, W.-P. & BRANDT, L. 2013 Active suspensions in thin films: nutrient uptake and swimmer motion. *J. Fluid Mech.* **733**, 528–557.

LAUGA, E. & POWERS, T.R. 2009 The hydrodynamics of swimming microorganisms. *Rep. Prog. Phys.* **72**, 096601.

LIGHTHILL, M.J. 1952 On the squirming motion of nearly spherical deformable bodies through liquids at very small Reynolds numbers. *Commun. Pure Appl. Maths* **5**, 109–118.

LOPEZ, D. & GUAZZELLI, E. 2017 Inertial effects on fibers settling in a vortical flow. *Phys. Rev. Fluids* **2**, 024306.

MARATH, N.K. & SUBRAMANIAN, G. 2018 The inertial orientation dynamics of anisotropic particles in planar linear flows. *J. Fluid Mech.* **844**, 357–402.

MEIBOHM, J., CANDELIER, F., ROSÉN, T., EINARSSON, J., LUNDELL, F. & MEHLIG, B. 2016 Angular velocity of a spheroid log rolling in a simple shear at small Reynolds number. *Phys. Rev. Fluids* **1**, 084203.

MENON, U., ROY, A., KRAMEL, S., VOTH, G. & KOCH, D. 2017 Theoretical predictions of the orientation distribution of high-aspect-ratio, inertial particles settling in isotropic turbulence. In *70th Annual Meeting of the APS Division of Fluid Dynamics*. Abstract Q36.00011.

PEDLEY, T.J. & KESSLER, J.O. 1987 The orientation of spheroidal microorganisms swimming in a flow field. *Proc. R. Soc. Lond.* B **231** (1262), 47–70.

PESKIN, C.S. 2002 The immersed boundary method. *Acta Numerica* **11**, 479–517.

QIU, J., CUI, Z., CLIMENT, E. & ZHAO, L. 2022 Gyrotactic mechanism induced by fluid inertial torque for settling elongated microswimmers. *Phys. Rev. Res.* **4** (2), 023094.

REDAELLI, T., CANDELIER, F., MEHADDI, R. & MEHLIG, B. 2022 Unsteady and inertial dynamics of a small active particle in a fluid. *Phys. Rev. Fluids* **7**, 044304.

ROBERTS, A.M. 1970 Geotaxis in motile micro-organisms. *J. Expl Biol.* **53**, 687–699.

ROBERTS, A.M. & DEACON, F.M. 2002 Gravitaxis in motile micro-organisms. *J. Fluid Mech.* **452**, 405–423.

ROSÉN, T., EINARSSON, J., NORDMARK, A., AIDUN, C.K., LUNDELL, F. & MEHLIG, B. 2015 Numerical analysis of the angular motion of a neutrally buoyant spheroid in shear flow at small Reynolds numbers. *Phys. Rev.* E **92**, 063022.

ROY, A., HAMATI, R.J., TIERNEY, L., KOCH, D.L. & VOTH, G.A. 2019 Inertial torques and a symmetry breaking orientational transition in the sedimentation of slender fibres. *J. Fluid Mech.* **875**, 576–596.

SMAYDA, T.J. 2010 Adaptations and selection of harmful and other dinoflagellate species in upwelling systems 1. Morphology and adaptive polymorphism. *Prog. Oceanogr.* **85** (1–2), 53–70.

SUBRAMANIAN, G. & KOCH, D.L. 2005 Inertial effects on fibre motion in simple shear flow. *J. Fluid Mech.* **535**, 383–414.

TITELMAN, J. & KIØRBOE, T. 2003 Motility of copepod nauplii and implications for food encounter. *Mar. Ecol. Prog. Ser.* **247**, 123–135.

UHLMANN, M. 2005 An immersed boundary method with direct forcing for the simulation of particulate flows. *J. Comput. Phys.* **209**, 448–476.

VESEY II, J. & GOLDENFELD, N. 2007 Simple viscous flows: from boundary layers to the renormalization group. *Rev. Mod. Phys.* **79**, 883–927.

VISSER, A. 2011 *Small, Wet and Rational, Individual Based Zooplankton Ecology*. DTU Denmark.

WANG, S. & ARDEKANI, A. 2012 Inertial squirmer. *Phys. Fluids* **24** (10), 101902.